Biomass Burning Aerosol as a Modulator of Droplet Number in the Southeast Atlantic Region

Mary Kacarab[1], K. Lee Thornhill[2], Amie Dobracki[3], Steven G. Howell[3], Joseph R. O'Brien[4], Steffen Freitag[3], Michael R. Poellot[4], Robert Wood[5], Paquita Zuidema[6], Jens Redemann[7], and Athanasios Nenes[1,8,9]

[1]School of Earth & Atmospheric Sciences, Georgia Institute of Technology, Atlanta, GA, 30332, USA
[2]NASA Langley Research Center, Hampton, VA, 23666, USA
[3]Department of Oceanography, University of Hawaii, Honolulu, HI, 96822, USA
[4]Atmospheric Sciences Department, University of North Dakota, Grand Forks, ND, 58202, USA
[5]Atmospheric Sciences, University of Washington, Seattle, WA, 98195, USA
[6]Department of Atmospheric Sciences, Rosenstiel School of Marine and Atmospheric Science, University of Miami, Miami, FL, 33149, USA
[7]School of Meteorology, University of Oklahoma, Norman, OK, 73072, USA
[8]Institue for Chemical Engineering Sciences, Foundation for Research and Technology Hellas, Patras, GR-26504, Greece
[9]Laboratory of Atmospheric Processes and their Impacts, School of Architecture, Civil and Environmental Engineering, Ecole Polytechnique Federale de Lausanne, Lausanne, CH-1015, Switzerland

Corresponding Author: Athanasios Nenes (athanasios.nenes@epfl.ch)

Abstract

The southeastern Atlantic (SEA) and its associated cloud deck, off the west coast of central Africa, is an area where aerosol-cloud interactions can have a strong radiative impact. Seasonally, extensive biomass burning (BB) aerosol plumes from southern Africa reach this area. The NASA ObseRvations of Aerosols above Clouds and their intEractionS (ORACLES) study focused on quantitatively understanding these interactions and their importance. Here we present measurements of cloud condensation nuclei (CCN) concentration, aerosol size distribution, and characteristic vertical updraft velocity (w^*) in and around the marine boundary layer (MBL) collected by the NASA P-3B aircraft during the August 2017 ORACLES deployment. BB aerosol levels vary considerably but systematically with time; high aerosol concentrations were observed in the MBL (800-1000 cm^{-3}) early on, decreasing mid-campaign to concentrations between 500-800 cm^{-3}. By late August and early September, relatively clean MBL conditions were sampled (<500 cm^{-3}). These data then drive a state-of-the-art droplet formation parameterization, from which the predicted cloud droplet number and its sensitivity to aerosol and dynamical parameters are derived. Droplet closure was achieved to within 20%. Droplet formation sensitivity to aerosol concentration, ~~vertical updraft velocity,~~w^*, and the hygroscopicity parameter, κ, vary and contribute to the total droplet response in the MBL clouds. When aerosol concentrations exceed ~900 cm^{-3} and maximum supersaturation approaches 0.1%, droplet formation in the MBL enters a "velocity-limited" droplet activation regime, where cloud droplet number responds weakly to CCN concentration increases. Below ~500 cm^{-3}, in a "clean" MBL, droplet formation is much more sensitive to changes in aerosol concentration than to changes in vertical updraft. In the "competitive" regime, where the

MBL has “intermediate” pollution (500-800 cm^{-3}), droplet formation becomes much more sensitive to hygroscopicity (κ) variations than for clean and polluted conditions. Higher concentrations increase the sensitivity to vertical velocity by more than ten-fold. We also find that characteristic vertical velocity plays a very important role in driving droplet formation in a more polluted MBL regime, in which even a small shift in w^* may make a significant difference in droplet concentrations. Identifying regimes where droplet number variability is primarily driven by updraft velocity and not aerosol concentration is key for interpreting aerosol indirect effects, especially with remote sensing. Droplet number responds proportionally to changes in characteristic velocity, offering the possibility of remote sensing of w^* under velocity-limited conditions.

1. Introduction

Aerosol particles affect the planetary radiative balance by directly absorbing and scattering radiation. They also provide the nuclei upon which cloud droplets and ice crystals form; variations thereof can profoundly impact cloud formation, precipitation, and the hydrological cycle (Boucher et al., 2013; Myhre et al., 2013). These aerosol impacts are thought to be important but uncertain modulators of regional and global scale climate. The interactions of aerosols with clouds are especially uncertain, and affect estimates of equilibrium climate sensitivity and transient climate response to greenhouse gas concentrations (Seinfeld et al., 2016, IPCC 2013).

Only a fraction of aerosol can affect clouds; those aerosols that can activate to form cloud droplets (termed cloud condensation nuclei, CCN) must satisfy a certain range of physical size and chemical composition for the levels of water vapor supersaturation that develop in cloud-forming air parcels (Köhler, 1936; Seinfeld and Pandis, 2006). The properties and dynamical development of warm and mixed-phase clouds are sensitive to the number of cloud droplets formed. It is now established that anthropogenic emissions have strongly modulated global CCN and droplet number since the industrial revolution (e.g., Boucher et al., 2013; Raatikainen et al., 2013). Much work remains, however, to reduce the uncertainty associated with this forcing on climate (e.g., Seinfeld et al., 2016).

Appropriately capturing the variability in droplet number, and its sensitivity to aerosol (which is at the heart of aerosol-cloud interactions) requires a good description of aerosol size distribution and hygroscopicity (e.g., Fanourgakis et al., 2019), especially in boundary-layer clouds where liquid clouds and their radiative cooling dominates. Key towards achieving this goal is to capture the source characteristics of major aerosol types,

and their chemical/microphysical evolution throughout their atmospheric residence. Biomass burning (BB) aerosol has emerged as a major source of regional and global aerosol, contributing up to 64% of global surface CCN concentrations (Spracklen et al., 2011). The influence of BB is expected to increase in importance as the combustion of biomass (natural and anthropogenic) is expected to accelerate in the future, especially in Africa, while anthropogenic emissions decrease (Bond, et al. 2013, Andela et al., 2017).

Almost one third of annual global biomass burning emissions originate from regional fires across the savannah and woodlands of sub-Saharan Africa, and one fourth originate from southern Africa (van der Werf et al., 2010). From approximately June until October, these intense BB emissions are subsequently transported over the southeast Atlantic (SEA) region (Adebiyi and Zuidema, 2016; Garstang et al., 1996), greatly elevating CCN levels above background concentrations (Ross, et al., 2003) and interacting with low-level marine boundary layer clouds that are abundant in the SEA (e.g., Seager et al., 2003; Grosvenor et al., 2018; Zuidema et al., 2018). The SEA experiences a structure transition from marine stratocumulus to trade wind cumulus clouds, so the coincidence of large BB aerosol plumes implies a potentially large role for aerosol-cloud interactions to affect cloud radiative properties over a globally-relevant system, potentially modulating the extent of each regime and the transition itself (Yamaguchi et al., 2015; Zhou et al., 2017). The microphysical influence of BB aerosol on clouds, however, is non-linear, as increasing aerosol levels enhance the competition of CCN for water vapor, to the point where droplet formation may be insensitive to CCN concentration level (e.g., Rissman et al., 2004; Ruetter et al., 2009; Bougiatioti, et al., 2016). Dynamical adjustments (primarily vertical velocity) may also respond to CCN and cloud droplet number changes - therefore

it is important to quantify all these links, as model-assessments of BB aerosol-cloud-climate interactions in the SEA critically rely on them. Constraints, however, on such links are virtually nonexistent for this region of the globe.

This study analyzes data collected in August 2017 on the NASA ObseRvations of Aerosols above CLouds and their intEractionS (ORACLES) campaign, and provides a systematic mapping of CCN concentration, aerosol size distribution, hygroscopicity, and cloud vertical velocity in the SEA. The in-situ measurements are then coupled with a state-of-the-art droplet parameterization to determine the in-cloud maximum supersaturation (S_{max}) achieved in the cloud updrafts and its response to aerosol changes. The data then is used to quantify the sensitivity of droplet formation to variations in vertical velocity and aerosol. We also explore whether the presence of BB aerosol correlates with shifts in the cloud vertical velocity driving droplet formation. These perturbations in BB aerosol availability, linked with vertical updraft dynamics, and predicted cloud droplet formation allow for understanding the drivers of droplet formation in the SEA cloud deck, and the degree to which BB influences droplet formation in the boundary layer.

2. Methods

2.1 Observational Data Set

A complete description and overview of the project is provided by Redemann, et al. (in preparation). All measurements were taken aboard the National Aeronautics and Space Administration (NASA) P-3B aircraft from August 12th through 31st as part of the ORACLES 2017 campaign. The aircraft was based at the International Airport (0.3778°N, 6.7131°E) of São Tomé, an island off the west coast of central Africa. A map of MODIS

satellite fires for the month of August 2017 can be found in Figure ~~S1~~1. The burning area is largely savanna grassland and the subsequent smoke plume travels westward over the SEA region. This work focuses on data collected on eight different research flights in the 2017 campaign during which instrumentation providing all relevant aerosol microphysical and cloud-scale dynamics data performed optimally. Flight paths for all data used in this work can be found in Figure 1. Most flights followed a "routine" route going out to 5°E longitude and then due South. Each flight included legs at varying altitudes to capture the characteristics of the plume, the marine boundary layer (MBL~~,~~), and the cloud deck. This work primarily focuses on the aerosol measured below-cloud in the MBL, as that is the aerosol that will participate in cloud droplet activation.

2.2 Instrumentation

A summary of the relevant measurements obtained at each flight can be found in Table 1. A solid diffuser inlet, characterized previously as having a 4μm dry diameter cut-off (McNaughton, et al. 2007), was used to sample aerosol onboard the aircraft. A Droplet Measurement Technologies (DMT; CCN-100) Continuous Flow Streamwise Thermal Gradient Chamber (CFSTGC; Roberts and Nenes, 2005) was used to measure CCN concentrations using a DMT constant pressure inlet operated at 600 mbar pressure. Since CCN measurements are highly sensitive to fluctuations in pressure and their effect on generated supersaturation (Raatikainen, et al. 2014), a flow orifice and active control system were used upstream of the instrument to ensure that the pressure remained constant, despite fluctuations in ambient pressure with altitude. The instrument was operated in both "standard" mode, where supersaturation (SS%) was stepped between 0.1, 0.2, and 0.3% by changing the temperature gradient in the droplet growth chamber, and in "scanning flow

CCN analysis" (SFCA) mode (Moore and Nenes, 2009), where supersaturation was varied from 0.1% to 0.4% by cycling the flow in a sinusoidal pattern from 300 to 1000 cm^3 min^{-1} while maintaining a constant temperature gradient in the growth chamber. Aerosol particles that activated into droplets sized greater than 0.5μm were then counted as CCN by the optical particle counter located at the exit of the CFSTGC growth chamber.

A DMT Ultra High Sensitivity Aerosol Spectrometer (UHSAS) was also operated on the same 600mbar constant pressure inlet as the CFSTGC to detect the aerosol concentration from 80 to 1000 nm (Table 1). Comparison of UHSAS with DMA distributions revealed that the UHSAS counting efficiency dropped below about 80 nm (Howell et al., in preparation), which should not strongly affect our subsequent analysis – as particles larger than 80nm diameter contribute the exclusive majority of CCN that activate into droplets for the conditions considered. The aerosol size distribution was combined with CCN measurements to calculate the hygroscopicity parameter, κ, of the observed aerosol (Petters and Kreidenweis, 2007), following a procedure adopted in numerous studies (e.g., Kalkavouras et al., 2019; Bougiatioti et al., 2016; Moore et al., 2011; Lathem et al., ~~2012~~2013) where integration of the particle size distribution from the largest resolved bin in the UHSAS down to a characteristic size, d_{crit} (also known as the "critical diameter"), matches the measured CCN concentration. The hygroscopicity then is obtained from from d_{crit} and the instrument supersaturation, following Kalkavouras et al. (2019).

Vertical winds on the P-3B were measured with the Turbulent Air Motion Measurement System (TAMMS) (Thornhill et al., 2003). Fast-response flow-angle, pressure, and temperature sensors combined with a GPS corrected inertial navigation

system (INS) provide 50 Hz inputs to compute 20 Hz averaged vertical winds via the full air motion equations from Lenschow (1986). The updraft velocities are then used as an input to calculate cloud droplet number concentration via a Gaussian distribution of updraft velocities (Section 2.3).

An Aerodyne High-Resolution Time-of-Flight Aerosol Mass Spectrometer (HR-ToF-AMS) (~~Jimenez~~DeCarlo, et al., 2006) was used to monitor bulk chemical composition of sampled aerosol throughout all flights. The bulk chemical composition acquired is then used to calculate the "bulk" κ (Petters and Kreidenweis, 2007), based on the mass fraction of organics and sulfate in the aerosol – assuming that the hygroscopicity of the organic fraction, κ_{org}=0.1, and of sulfate, $\kappa_{sulfate}$=0.6. We have also ignored the effects of insoluble material – such as black carbon – as it constitutes a small volume fraction of the aerosol and has a negligible influence on hygroscopicity. The bulk-derived κ allows for comparison with the directly calculated κ from the CFSTGC and UHSAS measurements, even if the AMS-derived values correspond to larger sizes than the CCN-derived κ. Nevertheless, strong agreement is found between the two κ values (Table 1; Figure S1), thus confirming that the internal mixture assumption inherent to CCN-derived hygroscopicity applies, and, that the composition varies little over the size range between d_{crit} (~100-200nm) and the peak of the mass distribution resolved by the AMS. It should also be noted that all of the AMS data was in high-sensitivity mode; the AMS heater was operated at an indicated 600 ^{o}C, which was tested and proved optimal for the ORACLES ~~BBOA~~BB Organic Aerosol plume. The data were processed using the standard AMS software (Squirrel, version 1.41).

A Droplet Measurement Technologies (DMT) Cloud Droplet Probe (CDP) was used to measure the cloud droplet number from 2 to 50 micron in diameter. The CDP was

modified according to Lance et al. (2010) to reduce coincidence problems. The total cloud droplet number (N_d) from the CDP is compared against the predicted N_d from the cloud droplet parameterization. These comparisons are done in flights with mostly stacked legs in the MBL and clouds; occasionally, flights where aerosol and cloud were immediately before or after each other were used (but not stacked).

2.3 Predicted Cloud Droplet Number

The droplet activation process is the direct microphysical link between clouds and aerosol. Every aerosol particle, to activate and form a cloud droplet, requires exposure to a "critical" supersaturation (or above) for enough time to grow past a "critical" wet size (Nenes et al., 2001) that ensures unconstrained growth. Applying this principle to ambient clouds is confounded by the complex relationship of supersaturation with aerosol size distribution, hygroscopicity, and the characteristic vertical updraft velocity. State-of-the-art cloud droplet parameterizations (e.g., Ghan et al., 2011; Morales and Nenes, 2014), however, resolve this relation and determine the cloud droplet number (N_d), maximum available supersaturation (S_{max}), and sensitivity of N_d to changes in aerosol concentration (N_a), vertical updraft velocity (w), and CCN activity (κ).

In this study, we utilize the Nenes and Seinfeld (2003) parameterization with improvements introduced by Fountoukis and Nenes (2005), Barahona et al., (2010) and Morales and Nenes (2014). In applying the droplet parameterization, we integrate over the distribution of vertical velocities within the boundary layer – by utilizing the "characteristic vertical velocity" approach of Morales and Nenes (2010). In this approach, instead of numerically integrating over a probability density distribution (PDF), the parameterization is applied at a "characteristic" velocity, w^*, that yields the same result as the integrated

value over the PDF. To derive w^*, the measured updrafts (positive vertical winds~~,~~), w, are taken from all segments just below cloud in a given flight, then fit to a Gaussian distribution with zero mean; $w^*=0.79\sigma_w$, where σ_w is the width of the vertical velocity spectrum (Morales and Nenes, 2010). ~~A consistency check~~Stratocumulus clouds, such as those sampled in this study, are well characterized by a Gaussian distribution of ~~the validity of the PDF, is that the mean velocity needs to be~~vertical velocities with a mean close to zero~~.~~ (Morales and Nenes, 2010). A comparison between the predicted N_d from the parameterization and the measured N_d from the CDP can be found in Figure S2. The parameterized N_d was, on average, within 20% of the measured N_d, which is within the ~~the~~ difference range of previous droplet closure studies (e.g., Meskhidze et al., 2005; Fountoukis et al., 2007; Morales et al., 2011).

3. Results and Discussion

3.1 Marine Boundary Layer Air Mass Characterization

Characteristic vertical profiles of CCN concentrations from 0.1 to 0.4% supersaturation for flights used in this work are shown in Figure 2. Earlier flights (RF01 – RF03) have lower BB plume heights, relatively little vertical variation of concentration within the plume, and high CCN concentrations in the marine boundary layer (MBL). Later flights (RF08 – RF12) show distinct layering in the plume, a higher plume cap altitude, and lower MBL concentrations. Hereon we focus on aerosol concentrations in the MBL, being the relevant aerosol providing CCN for BL cloud formation. A summary of the MBL aerosol concentrations, CCN~~–~~–derived κ (averaged over all the supersaturations measured), and characteristic vertical updraft velocity (w^*) is provided for all flights in Table 1. Flights

245 are classified according to the observed MBL aerosol concentrations from the UHSAS into
246 categories defined, for the purposes of this work, as *"*polluted*"* (exceeding 800 cm^{-3}),
247 *"*intermediate*"* (500-800 cm^{-3}), and *"*clean*"* (below 500 cm^{-3}). MBL aerosol concentration
248 is higher earlier on in August and decreases as the mission progresses. The average CCN-
249 derived κ for the MBL aerosol is fairly consistent, ranging from 0.2 to 0.4, and agrees well
250 with the κ estimated from the bulk MBL aerosol elemental composition as measured by
251 the aerosol mass spectrometer, implying that the aerosol is chemically uniform throughout
252 the ultrafine aerosol size range (Figure S1).
253 Characteristic vertical updrafts are higher earlier in August, averaging 0.4 ms^{-1}, and
254 decrease to around 0.3 ms^{-1} later in the campaign. A decrease in MBL aerosol concentration
255 is also seen during this time, with earlier flights seeing aerosol concentrations reaching up
256 to 1000 cm^{-3} and later decreasing to 200 cm^{-3}. The average BB plume aerosol
257 concentrations aloft range from around 1250 cm^{-3} to 3000 cm^{-3}, but show no distinct trends
258 throughout the month. However, an interesting trend can be found in comparing the
259 altitudes of the bottom of the BB plume and the top of the MBL cloud deck with the
260 characteristic vertical updraft velocities – a lower w^* of 0.3 ms^{-1} coincides with observation
261 of a clean, low-aerosol "gap" between the top of the MBL clouds and the bottom of the BB
262 plume. In higher w^* flights (0.4 ms^{-1}), the BB plume extends all the way down to the top
263 of the MBL cloud layers. In these flights, the BB plume is observed to have one single,
264 well-mixed layer throughout, while the later flights ($w^* \sim 0.3$ ms^{-1}) are characterized by
265 two distinct layers in the plume.
266
267 **3.2 Predicted Droplet Number and Maximum Supersaturation**

Figure 3a presents predicted droplet number (N_d) and CCN (at 0.1% supersaturation) as a function of total aerosol concentration (N_a) for the marine boundary layer (MBL) legs of all flights. Above an aerosol concentration of ~600 cm^{-3}, droplet number concentration becomes progressively less responsive to further increases in CCN number (as the incremental change in N_d is less as CCN increases) and becomes effectively insensitive ($\partial N_d/\partial N_a \sim 0$) for an aerosol concentration exceeding ~1000 cm^{-3}. The reason behind this increasing insensitivity can be seen in Figure 3b, which presents N_d against N_a for all the MBL leg data; the data are colored by supersaturation. For low values of N_a and N_d (~200cm^{-3}), S_{max} tends to be high (just over 0.2%) and the response of N_d to increases in aerosol is strong. However, when transitioning from "clean" to "intermediate" MBL conditions, N_d is less sensitive to increases in aerosol, because S_{max} decreases, and mitigates some of the expected droplet number response. Upon reaching "polluted" conditions ~~(~900~~(>800 cm^{-3}), the decrease in S_{max} is even stronger, entering into a regime where any additional aerosol can no longer substantially augment cloud droplets, owing to the extreme competition of the high CCN concentrations for water vapor. This water vapor-limited regime occurs when the S_{max} is less than 0.1% (Figure 3b); given that water vapor availability is generated through expansion cooling in updrafts, this type of limitation is also known as the "updraft-limited" regime of droplet formation (Ruetter et al., 2009).

3.3 Droplet Number Sensitivity

The previous section pointed out the variable sensitivity of droplet number to aerosol perturbations, depending on the conditions of cloud formation. To further explore such issues, we explicitly calculate the sensitivities (partial derivatives) of droplet number

291 in the MBL to changes in aerosol number, characteristic vertical updraft velocity, and CCN
292 activity, computed by the parameterization using a finite difference approximation. This is
293 shown in Figure 4 for $\partial N_d/\partial N_a$ (top panel), $\partial N_d/\partial w$ (middle panel) and $\partial N_d/\partial \kappa$ (bottom
294 panel). Results are shown for three flights, corresponding to each pollution class of Table
295 1: "polluted" (RF02), "intermediate" (RF09), and "clean" (RF10). Sensitivity of droplet
296 number to total aerosol concentration ($\partial N_d/\partial N_a$) is fairly comparable between the two lower
297 concentration conditions and approaches insensitivity ($\partial N_d/\partial dN_a < 0.1$) when the total
298 aerosol concentration exceeds 1000 cm^{-3}. Maximum in-cloud supersaturation decreases
299 steadily as N_a increases and $\partial N_d/\partial dN_a$ appreciably decreases when S_{max} drops below 0.12%
300 (Figure 4, top panel).
301 As $\partial N_d/\partial N_a$ decreases with increasing levels of aerosol, droplet sensitivity to
302 vertical updraft velocity, $\partial N_d/\partial w$, becomes increasingly important and completely
303 dominates droplet variability for high aerosol numbers. The reason why droplets become
304 so sensitive to vertical velocity fluctuations under polluted conditions, is because vertical
305 velocity drives supersaturation generation; at low supersaturation, when there is very
306 strong competition for water vapor from the many CCN present ("velocity-limited
307 regime"), any increase in vertical velocity augments supersaturation and droplet number.
308 For low CCN concentrations, however, supersaturation is high so that fluctuations in
309 aerosol translate to an almost equal response in droplet number ($\partial N_d/\partial dN_a \sim 1$; Figure 4,
310 top panel), therefore fluctuations in vertical velocity, hence supersaturation, do not affect
311 droplet number ($\partial N_d/\partial w$ small). The low MBL aerosol concentrations lead to the highest
312 sensitivity of N_d to N_a (approaching 100%), creating an "aerosol-limited" condition where
313 there is sufficient available supersaturation to activate virtually every aerosol added to the

MBL layer. A ~5x increase in N_a leads to a ~50% decrease in the sensitivity of N_d to N_a to around 40%, with the highest aerosol values corresponding to even lower sensitivities to aerosol number, approaching below 10% and clearly behavior consistent with a "velocity-limited" regime.

Predicted droplet sensitivity to κ displays a unique trend (Figure 4, bottom panel), becoming stronger initially with increasing aerosol, peaking at intermediate concentrations and then rapidly dropping towards insensitivity, when supersaturation approaches 0.1%. This sudden insensitivity to CCN activity aligns with the clouds being overseeded when supersaturation is starting to be depleted – once supersaturation is not as readily available, any characteristics of the aerosol cease to play a strong role in activation. However, prior to reaching the point of being insensitive to aerosol, increased sensitivity to κ is opposite to the expected trend from N_a – indicating that the fluctuation in chemical composition, when droplet formation is in a "competitive" regime (Figure 4c), may be an important contributor to droplet formation – consistent with the findings of Bougiatioti et al., (2017) for droplet formation in an urban environment in the E. Mediterranean. We emphasize here that the sensitivity to κ (Figure 4c) is not from its changes over size (which we show above to be small), but rather changes over space and time.

3.2.1 Impact of Boundary Layer Turbulence

Throughout the entirety of flights, the maximum predicted droplet number reaches a plateau, where additional aerosol does not result in any significant increase in N_d. An example of this behavior is presented in Supplementary Figure S4 (where data of calculated N_d is presented for the entire research flight, as opposed to only the segments in the MBL

shown in previous sections). This plateau, owing to the development of strong water vapor limitations, is termed limiting droplet number, N_d^{lim}, and should largely be a function of vertical velocity – precisely because we are in a velocity-limited regime. This realization implies that much of the droplet number variability (measured or retrieved) in clouds strongly influenced by BB plumes reflects the underlying shifts in cloud dynamics associated with each concentration "regime". Indeed, the characteristic velocity in the MBL tends to increase as the MBL clouds become progressively polluted (Figure 5); the higher pollution flights (RF01 and RF02) all fall in mid-August and are coincident with a higher characteristic vertical updraft velocity of ~ 0.4, while "clean" MBL flights coincide with lower vertical updraft velocity values of ~0.3 and occur towards the end of August. "Intermediate" scenario flights are divided between the two characteristic vertical updraft velocities observed. When the flight-specific characteristic velocity is then used to calculate the droplet response, it follows a trend with aerosol levels that magnifies droplet response from what is expected by increasingly adding pollution alone. In contrast, the aerosol concentration above the MBL is inversely correlated with w^* (Figure 5), possibly a result of enhanced mixing between the MBL and the free troposphere (rich in BB aerosol) that is associated with the elevated levels of turbulence (w^*).

The impact of increased w^* on the droplet number is shown for "polluted", "intermediate" and "clean" conditions in the inset plot of Figure ~~5~~6 – which shows N_d^{lim} for each concentration class for w^* between 0.1 and 0.6 ms^{-1}. For polluted conditions, transitioning from 0.3 to 0.4 ms^{-1} increases droplet number from 400 to 500 cm^{-3}, which is a 20-25% increase. The enhancement is equally important for intermediate and clean

conditions (although less in absolute number), and always comparable to droplet enhancements from changes in BB concentration.

3.4 Water-vapor limitations and the lifetime of BB aerosol in the MBL

Above an aerosol concentration of ~800 cm^{-3} when water vapor availability is severely limited, N_d no longer increases in response to increases in CCN (Figure 3a). An important consequence is that under such conditions, much of the BBOA does not activate into cloud droplets and is therefore not lost through wet deposition. Because of this, the degree of water vapor competition (and supersaturation level) is directly related to BB lifetime in the MBL ~~(Figure 9).~~ $\partial N_d/\partial dN_a$ may then be inversely linked to CCN lifetime, where "velocity-limited" conditions, characterized by the smallest droplet activation fraction and $\partial N_d/\partial dN_a$, also have the largest lifetime and vice versa for "clean" MBL conditions.

Formatted: Indent: First line: 0"

4. Implications and Conclusions

BB aerosol levels in the SEA varied considerably throughout the 2017 ORACLES deployment. Earlier in the campaign, high aerosol concentrations were observed in the MBL (800-1000 cm^{-3}), which decreased mid-campaign to concentrations between 500-800 cm^{-3}, and in late August and early September, relatively clean MBL conditions were seen (<500 cm^{-3}). On 12-13 August, MBL aerosol concentrations exceeded 1000 cm^{-3}. From the observed aerosol size distribution and CCN concentrations, we constrained the aerosol hygroscopicity – which was in agreement with estimates from bulk chemical composition

382 measurements; together with observed MBL vertical velocity distributions, we then
383 calculate droplet number concentrations using a state-of-the-art droplet activation
384 parameterization. Droplet closure was achieved within 20%, consistent with the degree of
385 closure achieved in past studies.

386 From the analysis of the dataset, when aerosol concentrations exceed ~900 cm^{-3}
387 and maximum supersaturation approaches 0.1%, droplet formation in the MBL begins to
388 enter a "velocity-limited" droplet activation regime, where cloud droplet number responds
389 weakly to CCN concentration increases. Lower MBL concentrations (500 cm^{-3} or less)
390 were observed later in the campaign (late August to early September), thus leading to a
391 much higher predicted S_{max} of 0.2%, and much higher fraction of activated CCN. Under
392 clean conditions, vertical velocity generates ample supersaturation, so droplet formation is
393 limited by the number of aerosol particles in the MBL. Overall this leads to a buffering of
394 the N_d response to aerosol, so that N_d variability is much less (down to 1/10 or less) than
395 that seen for the underlying CCN.

396 Droplet formation sensitivity to aerosol concentration, vertical updraft velocity, and
397 the hygroscopicity parameter, κ, vary and contribute to the total droplet response in the
398 MBL clouds. Droplet sensitivity to vertical velocity increases an order of magnitude as
399 aerosol concentration reaches 1000 cm^{-3}. This highlights the increased (and eventually
400 dominant) role that vertical velocity plays in droplet formation in a "polluted" MBL
401 environment. Below ~500 cm^{-3}, in a "clean" MBL, droplet formation is much more
402 sensitive to changes in aerosol concentration than to the observed changes in vertical
403 updrafts. In the "competitive" regime, where the MBL has "intermediate" pollution (500-
404 800 cm^{-3}), hygroscopicity (κ) variations emerges as an important driver of droplet number

405 variability, which is something not seen for either "clean" or "polluted" MBL conditions.
406 Throughout the month of August, a shift is observed in w^*, from ~0.45 m s^{-1} down to ~0.26
407 m s^{-1}, which affects the maximum droplet number that can be generated in the MBL. N_d^{lim}
408 is significantly affected by changes in w^*, especially in higher MBL pollution conditions,
409 where the effects of increased characteristic vertical updraft velocity significantly
410 magnifies droplet number concentrations compared to trends seen in "intermediate" and
411 "clean" MBL environments.

412 Identifying regimes where droplet number variability is primarily driven by updraft
413 velocity changes, and not aerosol concentration, is key for interpreting aerosol indirect
414 effects. This is particularly important when using remote sensing data, as can be seen from
415 the data here: diagnosing aerosol indirect effects using above-cloud aerosol would give
416 opposite trends from what actually occurs in the MBL – because BB plume aerosol
417 decreases as the MBL aerosol increases. Nevertheless, the correlations here between
418 above-cloud and MBL aerosol level might be a useful way to diagnose MBL aerosol –
419 from which N_d can eventually be determined. Furthermore, when droplet number is in the
420 velocity-limited regime, N_d responds proportionally to changes in w^*, offering the
421 possibility of remote sensing of w^* under these specific conditions (specific criteria need
422 to be developed to help define when velocity-limited conditions occur, e.g., combining
423 collocated in-situ and remote sensing data from field intensives).

424 Very interesting are the trends observed between MBL dynamics, height and the
425 aerosol levels in the MBL and the BB plume. w^* is higher earlier in August and decreases
426 later in the campaign; MBL aerosol concentration correlates with w^*, while an inverse
427 correlation is seen for the aerosol in the BB plume above the MBL. A similarly interesting

trend can be found between w^*, the base altitude of the BB plume and the top of the MBL cloud deck: higher w^* corresponds to a BB plume that extends down to the top of the MBL cloud layers, while lower w^* is characterized by two distinct layers in the plume. Although what drives these correlations is not fully understood, it is likely related to the seasonality of the MBL height and its role in regulating mixing between the MBL and aloft (also discussed in Zhang et al., ~~2018~~2019). Indeed, the atmosphere is likely less stable in August, encouraging buoyant parcels (hence larger w^*) than in September. w^* enhancement may also result from enhanced cloud-top radiative cooling driven by LWC changes between the early and later flights of the campaign – the nearly threefold increase in cloud droplet number and the expected LWC response, however, suggests that clouds may actually be thinner (Painemal and Zuidema, 2010; Wood et al., 2012; de Szoeke et al., ~~2018).~~2018). Water vapor in the FT, which is strongly correlated with smoke occurrence in the FT, would also reduce the longwave emission from the top of the stratocumulus and thereby reduce the turbulent driving of the PBL. Water vapor in the outflow layers is driven by the proximity of the continental PBL to the warm continental surface with enhanced evaporation – and is not related to aerosol processes. Absorption of solar radiation from black carbon in the MBL may also suppress turbulence and w^* (Wilcox et al., 2016), although our data suggests these effects may not be strong enough to reverse the trend imposed by any MBL seasonality. A thorough attribution of the link between w^*, aerosol, MBL structure and the large scale remains to be carried out, though results here suggest simple thresholds on these variables could help models determine how to treat droplet activation in different scenarios.

Although BB aerosol variations can profoundly impact cloud microphysical characteristics, concurrent variations in vertical velocity must also be considered to fully understand the drivers of droplet variability, especially when used to evaluate models and estimates of aerosol-cloud-climate interactions. The small activation fraction of aerosols under polluted MBL conditions may promote the persistence of aerosol for longer in the MBL, extending the reach and influence of BB aerosol in the SEA.

Formatted: Font: Bold

Acknowledgements

MK and ~~TN~~AN gratefully acknowledge funding from NASA ORACLES grant NNX15AL68G and the European Research Council, CoG-2016 project PyroTRACH (726165) funded by H2020-EU.1.1. – Excellent Science. All other authors acknowledge support from the NASA EVS-2 program for their individual ORACLES grants. All ORACLES datasets are publicly available through doi: 10.5067/Suborbital/ORACLES/P3/2017_V1

Code/Data availability

The droplet parameterization used for the calculations in the study is available from the athanasios.nenes@epfl.ch upon request. ORACLES mission data can be downloaded from http://espoarchive.nasa.gov/archive/browse/oracles.

Author contribution

~~conceptualization~~Conceptualization, M.K. and A.N.; methodology, M.K. and A.N.; software, A.N.; formal analysis, M.K., A.N., S.H.; investigation, ~~A.B~~M.K. and A.N.; writing—original draft preparation, M.K. and A.N.; writing—review and editing: all authors.

Competing interests

The authors declare no competing interests.

References

Adebiyi, A. A., and Zuidema, P.: The role of the southern African easterly jet in modifying the southeast Atlantic aerosol and cloud environments, *Q.J.R. Meteorol. Soc.*, 142, 1574-1589. doi:10.1002/qj.2765, 2016.

Albrecht, B. A.: Aerosols, Cloud Microphysics, and Fractional Cloudiness, *Science*, 245, 4923, 1227-1230, doi:10.1126/science.245.4923.1227, 1989.

Andela, N., Morton, D. C., Giglio, L., Chen, Y., van der Werf, G. R., Kasibhatla, P. S., DeFries, R. S., Collatz, G. J., Hantson, S., Kloster, S., Bachelet, D., Forrest, M., Lasslop, G., Li, F., Mangeon, S., Melton, J. R., Yue, C., Randerson, J. T.: A human-driven decline in global burned area, *Science*, 356, 6345, 1356-1362, doi: 10.1126/science.aal4108, 2017.

Barahona, D., West, R. E. L., Stier, P., Romakkaniemi, S., Kokkola, H., and Nenes, A.: Comprehensively accounting for the effect of giant CCN in cloud activation parameterizations, *Atmos. Chem. Phys.,* 10, 2467-2473, https://doi.org/10.5194/acp-10-2467-2010, 2010.

~~Bond et al 2013~~ Bond, T. C., Doherty, S. J., Fahey, D. W., Forster, P. M., Berntsen, T., DeAngelo, B. J., Flanner, M. G., Ghan, S., Kärcher, B., Koch, D., Kinne, S., Kondo, Y., Quinn, P. K., Sarofim, M. C., Schultz, M. G., Schulz, M., Venkataraman, C., Zhang, H., Zhang, S., Bellouin, N., Guttikunda, S. K., Hopke, P. K., Jacobson, M. Z., Kaiser, J. W., Klimont, Z., Lohmann, U., Schwarz, J. P., Shindell, D., Storelvmo, T., Warren, S. G., Zender, C. S.: Bounding the role of black carbon in the climate system: A scientific assessment, *J. Geophys. Res.*, 118, 5380– 5552, doi:10.1002/jgrd.50171, 2013.

Boucher, O., Randall, D., Artaxo, P., Bretherton, C., Feingold, G., Forster, P., Kerminen, V.-M., Kondo, Y., Liao, H., Lohmann, U., Rasch, P., Satheesh, S. K., Sherwood, S., Stevens, B., and Zhang, X. Y.: Clouds and aerosols. In *Climate Change 2013: The Physical Science Basis. Contribution of Working Group I to the Fifth Assessment Report of the Intergovernmental Panel on Climate Change*. T.F. Stocker, D. Qin, G.-K. Plattner, M. Tignor, S.K. Allen, J. Doschung, A. Nauels, Y. Xia, V. Bex, and P.M. Midgley, Eds. Cambridge University Press, pp. 571-657, doi:10.1017/CBO9781107415324.016, 2013.

Bougiatioti, A., Bezantakos, S., Stavroulas, I., Kalivitis, N., Kokkalis, P., Biskos, G., Mihalopoulos, N., Papayannis, A., and Nenes, A.: Biomass-burning impact on CCN number, hygroscopicity and cloud formation during summertime in the eastern Mediterranean, *Atmos. Chem. Phys.*, 16, 7389-7409, doi:10.5194/acp-16-7389-2016, 2016.

Bougiatioti, A., Argyrouli, A., Solomos, S., Vratolis, S., Eleftheriadis, K., Papayannis, A., and Nenes, A.: CCN Activity, Variability and Influence on Droplet Formation during the HygrA-Cd Campaign in Athens. *Atmosphere*, 8, 108, 2017.

Cubison, M. J., Ervens, B., Feingold, G., Docherty, K. S., Ulbrich, I. M., Shields, L., Prather, K., Hering, S., and Jimenez, J. L.: The influence of chemical composition and mixing state of Los Angeles urban aerosol on CCN number and cloud properties, *Atmos. Chem. Phys.*, 8, 5649-5667, doi:10.5194/acp-8-5649-2008, 2008.

DeCarlo, P.F., J.R. Kimmel, A. Trimborn, M.J. Northway, J.T. Jayne, A.C. Aiken, M. Gonin, K. Fuhrer, T. Horvath, K. Docherty, D.R. Worsnop, and J.L. Jimenez: Field-Deployable, High-Resolution, Time-of-Flight Aerosol Mass Spectrometer, Analytical Chemistry, 78: 8281-8289, 2006.

de Szoeke, S. P., Verlinden, K. L., and Covert, D.: Cloud-scale droplet number sensitivity to liquid water path in marine stratocumulus. *J.Geoph.Res*, 123, 5320–5334, doi: 10.1029/2017JD027508, 2018.

Dusek, U., Frank, G. P., Hildebrandt, L., Curtius, J., Schneider, J., Walter, S., Chand, D., Drewnick, F., Hings, S., Jung, D., Borrmann, S., and Andreae, M. O.: Size Matters More Than Chemistry for Cloud-Nucleating Ability of Aerosol Particles, *Science*, 312:578, 1375-1378, 2006.

Fanourgakis, G. S., Kanakidou, M., Nenes, A., Bauer, S. E., Bergman, T., Carslaw, K. S., Grini, A., Hamilton, D. S., Johnson, J. S., Karydis, V. A., Kirkevåg, A., Kodros, J. K., Lohmann, U., Luo, G., Makkonen, R., Matsui, H., Neubauer, D., Pierce, J. R., Schmale, J., Stier, P., Tsigaridis, K., van Noije, T., Wang, H., Watson-Parris, D., Westervelt, D. M., Yang, Y., Yoshioka, M., Daskalakis, N., Decesari, S., Gysel-Beer, M., Kalivitis, N., Liu, X., Mahowald, N. M., Myriokefalitakis, S., Schrödner, R., Sfakianaki, M., Tsimpidi, A. P., Wu, M., and Yu, F.: Evaluation of global simulations of aerosol particle and cloud condensation nuclei number, with implications for cloud droplet formation, *Atmos. Chem. Phys.*, 19, 8591-8617, https://doi.org/10.5194/acp-19-8591-2019, 2019.

Fountoukis, C., and Nenes, A.: Continued development of a cloud droplet formation parameterization for global climate models, *J. Geophys. Res.*, 110, D11212, doi:10.1029/2004JD005591, 2005.

Fountoukis, C., Nenes, A., Meskhidze, N., Bahreini, R., Brechtel, F., Conant, W. C., Jonsson, H., Murphy, S., Sorooshian, A., Varutbangkul, V., R. C. Flagan, and J. H. Seinfeld: Aerosol–cloud drop concentration closure for clouds sampled during ICARTT, *J.Geoph.Res.*, 112, D10S30, doi:10.1029/2006JD007272, 2007.

Garstang, M., Tyson, P. D., Swap, R., Edwards, M., Kållberg, P., and Lindesay, J. A.: Horizontal and vertical transport of air over southern Africa, *J. Geophys. Res.*, 101(D19), 23721– 23736, doi:10.1029/95JD00844, 1996.

Ghan, S. J., Abdul-Razzak, H., Nenes, A., Ming, Y., Liu, X., Ovchinnikov, M., Shipway, B., Meskhidze, N., Xu, J., and Shi, X.: Droplet nucleation: Physically-based parameterizations and comparative evaluation, *J. Adv. Model. Earth Syst.*, 3, M10001, doi:10.1029/2011MS000074, 2011.

Grosvenor, D. P., Sourdeval, O.,Zuidema, P., Ackerman, A.,Alexandrov, M. D., Bennartz, R.,et al.: Remote sensing ~~ofdroplet~~of droplet number concentration ~~inwarm~~in warm clouds: A review of the currentstate of knowledge and perspectives, *Rev.Geoph*, 56, 409–453, doi:10.1029/2017RG000593, 2018.

Howell, et al., in prep.

Formatted: Font: Not Bold

IPCC, 2013: Climate Change 2013: The Physical Science Basis. Contribution of Working Group I to the Fifth Assessment Report of the Intergovernmental Panel on Climate Change [Stocker, T.F., D. Qin, G.-K. Plattner, M. Tignor, S.K. Allen, J. Boschung, A. Nauels, Y. Xia, V. Bex and P.M. Midgley (eds.)]. Cambridge University Press, Cambridge, United Kingdom and New York, NY, USA, 1535 pp, doi:10.1017/CBO9781107415324.

~~DeCarlo, P.F., J.R. Kimmel, A. Trimborn, M.J. Northway, J.T. Jayne, A.C. Aiken, M. Gonin, K. Fuhrer, T. Horvath, K. Docherty, D.R. Worsnop, and J.L. Jimenez: Field-Deployable, High-Resolution, Time-of-Flight Aerosol Mass Spectrometer, Analytical Chemistry, 78: 8281-8289, 2006.~~

Kalkavouras, P., Bougiatioti, A., Kalivitis, N., Tombrou, M., Nenes, A., and Mihalopoulos, N.: Regional New Particle Formation as Modulators of Cloud Condensation Nuclei and Cloud Droplet Number in the Eastern Mediterranean, *Atmos. Chem. Phys.*, 19, 6185-6203, https://doi.org/10.5194/acp-19-6185-2019, 2019

Kanakidou, M., Seinfeld, J. H., Pandis, S. N., Barnes, I., Dentener, F. J., Facchini, M. C., Van Dingenen, R., Ervens, B., Nenes, A., Nielsen, C. J., Swietlicki, E., Putaud, J. P., Balkanski, Y., Fuzzi, S., Horth, J., Moortgat, G. K., Winterhalter, R., Myhre, C. E. L., Tsigaridis, K., Vignati, E., Stephanou, E. G., and Wilson, J.: Organic aerosol and global climate modelling: a review, *Atmos. Chem. Phys.*, 5, 1053-1123, doi:10.5194/acp-5-1053-2005, 2005.

Kerminen, V.-M., Paramonov, M., Anttila, T., Riipinen, I., Fountoukis, C., Korhonen, H., Asmi, E., Laakso, L., Lihavainen, H., Swietlicki, E., Svenningsson, B., Asmi, A., Pandis, S. N., Kulmala, M., and Petäjä, T.: Cloud condensation nuclei production associated with atmospheric nucleation: a synthesis based on existing literature and new results, *Atmos. Chem. Phys.*, 12, 12037-12059, doi:10.5194/acp-12-12037-2012, 2012.

Klein, S. A., and Hartmann, D. L.: The Seasonal Cycle of Low Stratiform Clouds. *J. Climate*, 6, 1587–1606, doi:10.1175/1520-0442(1993)006<1587:TSCOLS>2.0.CO;2, 1993.

Kohler, H.: The nucleus in and the growth of hygroscopic droplets, *Trans Farad Soc*, 32, 1152–1161, 1936.

Lance, S., Brock, C. A., Rogers, D., and Gordon, J. A.: Water droplet calibration of the Cloud Droplet Probe (CDP) and in-flight performance in liquid, ice and mixed-phase clouds during ARCPAC, Atmos. Meas. Tech., 3, 1683–1706, ~~https://doi.org/10.5194/amt-3-1683-2010,~~https://doi.org/10.5194/amt-3-1683-2010, 2010.

Lathem, T.L., A.J. Beyersdorf, K.L. Thornhill, E.L. Winstead, M.J. Cubison, A. Hecobian, J.L. Jimenez, R.J. Weber, B.E. Anderson, and Nenes, A.: Analysis of CCN activity of Arctic aerosol and Canadian biomass burning during summer 2008, *Atmos.Chem.Phys.*, 13, 2735-2756, 2013.

Lenschow, D.H., ed. 1986: *Probing the Atmospheric Boundary Layer*. Amer. Meteorol. Soc.

Formatted: Font: Not Bold

Formatted: Font: Not Bold

McNaughton, C. S., Clarke, A. D., Howell, S. G., Pinkerton, M., Anderson, B., Thornhill, L., Hudgins, C., Winstead, E., Dibb, J. E., Scheuer, E., and Maring, H.: Results from the DC-8 Inlet Characterization Experiment (DICE): Airborne Versus Surface Sampling of Mineral Dust and Sea Salt Aerosols, *Aero. Sci. Tech.*, 41:2, 136-159, doi:10.1080/02786820601118406, 2007.

Meskhidze, N., ~~A.~~ Nenes, A., Conant, W. C., and Seinfeld, J.H.: Evaluation of a new Cloud Droplet Activation Parameterization with In Situ Data from CRYSTAL-FACE and CSTRIPE, *J.Geoph.Res.*, 110, D16202, doi:10.1029/2004JD005703, 2005.

Meyer, K., Platnick, S., and Zhang, Z.: Simultaneously inferring above-cloud absorbing aerosol optical thickness and underlying liquid phase cloud optical and microphysical properties using MODIS, J. Geophys. Res. Atmos., 120, 5524–5547, doi:10.1002/2015JD023128, 2015.

Moore, R. H., and Nenes, A.: Scanning Flow CCN Analysis—A Method for Fast Measurements of CCN Spectra, *Aero. Sci. Tech.*, 43:12, 1192-1207, doi:10.1080/02786820903289780, 2009.

Moore, R.H., Bahreini, R., Brock, C.A., Froyd, K.D., Cozic, J., Holloway, J.S., Middlebrook, A.M., Murphy, D.M., Nenes, A.: Hygroscopicity and Composition of Alaskan Arctic CCN During April 2008, *Atmos.Chem.Phys.*, 11, 11807-11825, 2011.

Morales, R., and Nenes, A.: Characteristic updrafts for computing distribution-averaged cloud droplet number and stratocumulus cloud properties, *J. Geophys. Res.*, 115, D18220, doi:10.1029/2009JD013233, 2010.

Morales, R., Nenes, A., Jonsson, H., Flagan, R.C. and J.H. Seinfeld: Evaluation of a diabatic droplet activation parameterization using in-situ cloud data, *J.Geoph.Res.*, 116, D15205, doi:10.1029/2010JD015324, 2011.

Morales Betancourt, R. and Nenes, A.: Understanding the contributions of aerosol properties and parameterization discrepancies to droplet number variability in a global climate model, *Atmos. Chem. Phys.*, 14, 4809-4826, doi:10.5194/acp-14-4809-2014, 2014.

~~Morales, R., Nenes, A., Jonsson, H., Flagan, R.C. and J.H. Seinfeld: Evaluation of a diabatic droplet activation parameterization using in-situ cloud data, *J.Geoph.Res.*, 116, D15205, doi:10.1029/2010JD015324, 2011.~~

Myhre, G., Samset, B. H., Schulz, M., Balkanski, Y., Bauer, S., Berntsen, T. K., Bian, H., Bellouin, N., Chin, M., Diehl, T., Easter, R. C., Feichter, J., Ghan, S. J., Hauglustaine, D., Iversen, T., Kinne, S., Kirkevåg, A., Lamarque, J.-F., Lin, G., Liu, X., Lund, M. T., Luo, G., Ma, X., van Noije, T., Penner, J. E., Rasch, P. J., Ruiz, A., Seland, Ø., Skeie, R. B., Stier, P., Takemura, T., Tsigaridis, K., Wang, P., Wang, Z., Xu, L., Yu, H., Yu, F., Yoon, J.-H., Zhang, K., Zhang, H., and Zhou, C.: Radiative forcing of the direct aerosol effect from AeroCom Phase II simulations, *Atmos. Chem. Phys.*, 13, 1853-1877, doi:10.5194/acp-13-1853-2013, 2013.

Formatted: Font: Not Bold

Formatted: Font: Not Bold

Formatted: Font: Not Bold

Formatted: Font: Not Bold

Nenes., A., Ghan, S., Abdul-Razzak, H., Chuang, P.Y., Seinfeld, J.H.: Kinetic Limitations on Cloud Droplet Formation and Impact on Cloud Albedo, *Tellus*, *53B*, 133-149, 2001

Nenes, A., and Seinfeld, J. H.: Parameterization of cloud droplet formation in global climate models, *J. Geophys. Res.*, 108, 4415, doi:10.1029/2002JD002911, D14, 2003.

Petters, M. D. and Kreidenweis, S. M.: A single parameter representation of hygroscopic growth and cloud condensation nucleus activity, *Atmos. Chem. Phys.*, 7, 1961-1971, doi:10.5194/acp-7-1961-2007, 2007.

Petters, M. D. and Kreidenweis, S. M.: A single parameter representation of hygroscopic growth and cloud condensation nucleus activity – Part 2: Including solubility, *Atmos. Chem. Phys.*, 8, 6273-6279, doi:10.5194/acp-8-6273-2008, 2008.

Painemal, D. and Zuidema, P.: Microphysical variability in Southeast Pacific stratocumulus clouds: Synoptic conditions and radiative response, Atmos. Chem. Phys., 10, 6255-6269. doi:10.5194/acp-10-6255-2010, 2010.

Pósfai, M., Simonics, R., Li, J., Hobbs, P. V., and Busek, P. R.: Individual aerosol particles from biomass burning in southern Africa: 1. Compositions and size distributions of carbonaceous particles, *J. Geophys. Res.*, 108, 8483, doi:10.1029/2002JD002291, D13, 2003.

Raatikainen, ~~T., Lin, J. J., Cerully, K. M., Lathem, T. L., Moore, R. H., and Nenes, A.: CCN Data Interpretation Under Dynamic Operation Conditions, *Aero. Sci. Tech.*, 48:5, 552-561, doi:10.1080/02786826.2014.899429, 2014.~~

~~Raatikainen,~~T., Nenes,A., Seinfeld, J. H., Morales,R., Moore, R. H., Lathem, T. L., Lance, S., Padro, L. T., Lin, J. J., Cerully, K., Bougiatioti, A., Cozic, J., Ruehl, C., Chuang, P. Y., Anderson, B., Flagan, R.C., Jonsson, H., Mihalopoulos, N., and J. N. Smith: Worldwide data sets constrain the water vapor uptake coefficient in cloud formation, *Proc.Nat.Acad.Sci.*, doi: 10.1073/pnas.1219591110, 2013.

Raatikainen, T., Lin, J. J., Cerully, K. M., Lathem, T. L., Moore, R. H., and Nenes, A.: CCN Data Interpretation Under Dynamic Operation Conditions, *Aero. Sci. Tech.*, 48:5, 552-561, doi:10.1080/02786826.2014.899429, 2014.

Redemann, J., et al.: An overview of the ORACLES (ObseRvations of Aerosols above CLouds and their intEractionS) project: aerosol-cloud-radiation interactions in the Southeast Atlantic basin, in preparation.

Rissman, T., Nenes, A., and Seinfeld, J. H.: Chemical amplification (or dampening) of the Twomey effect: Conditions derived from droplet activation theory, *J. Atmos. Sci.*, 61, 919–930, 2004.

Reutter, P., Su, H., Trentmann, J., Simmel, M., Rose, D., Gunthe, S. S., Wernli, H., Andreae, M. O., and Pöschl, U.: Aerosol- and updraft-limited regimes of cloud droplet formation: influence of particle number, size and hygroscopicity on the activation of cloud

condensation nuclei (CCN), *Atmos. Chem. Phys.*, 9, 7067-7080, https://doi.org/10.5194/acp-9-7067-2009, 2009

Roberts, G. C., and Nenes, A.: A Continuous-Flow Streamwise Thermal-Gradient CCN Chamber for Atmospheric Measurements, *Aero. Sci. Tech.*, 39:3, 206-221, doi:10.1080/027868290913988, 2005.

Ross, K. E., Piketh, S. J., Bruintjes, R. T., Burger, R. P., Swap, R. J., and Annegarn, H. J.: Spatial and seasonal variations in CCN distribution and the aerosol-CCN relationship over southern Africa, *J. Geophys. Res.*, 108, 8481, doi:10.1029/2002JD002384, D13, 2003.

Seager, R., Murtugudde, R., Naik, N., Clement, A., Gordon, N., & Miller, J.: Air–Sea Interaction and the Seasonal Cycle of the Subtropical Anticyclones. *J. Climate*, 16, 1948-1966, 2003.

Seinfeld, J.H. and Pandis, S.N.: Atmospheric Chemistry and Physics: From Air Pollution to Climate Change. 2nd Edition, John Wiley & Sons, New York, 2006.

Seinfeld, J. H., Bretherton, C., Carslaw, K. S., Coe, H., DeMott, P. J., Dunlea, E. J., Feingold, G., Ghan, S., Guenther, A. B., Kahn, R., Kraucunas, I., Kreidenweis, S. M., Molina, M. J., Nenes, A., Penner, J. E., Prather, K. A., Ramanathan, V., Ramaswamy, V., Rasch, P. J., Ravishankara, A. R., Rosenfeld, D., Stephens, G., and Wood, R.: Improving our fundamental understanding of the role of aerosol−cloud interactions in the climate system, *Proc.Nat.Acad.Sci.*, 113 (21) 5781-5790; doi:10.1073/pnas.1514043113, 2016.

Sinha, P., Hobbs, P. V., Yokelson, R. J., Bertschi, I. T., Blake, D. R., Simpson, I. J., and Gao, S.: Emissions of trace gases and particles from savanna fires in southern Africa, *J. Geophys. Res.*, 108, 8487, doi:10.1029/2002JD002325, D13, 2003.

Spracklen, D. V., Carslaw, K. S., Pöschl, U., Rap, A., and Forster, P. M.: Global cloud condensation nuclei influenced by carbonaceous combustion aerosol, *Atmos. Chem. Phys.*, 11, 9067-9087, doi:10.5194/acp-11-9067-2011, 2011.

Thornhill, K. L., Anderson, B. E., Barrick, J. D. W., Bagwell, D. R., Friesen, R., and Lenschow, D.: Air motion intercomparison flights during Transport and Chemical Evolution in the Pacific (TRACE-P)/ACE-ASIA. Journal of Geophysical Research. 108. 10.1029/2002JD003108, 2003.

Twomey, S.: Pollution and the Planetary Albedo, *Atmos. Env.*, 8, 1251-1256, doi:10.1016/0004-6981(74)90004-3, 1974.

Twomey, S.: The Influence of Pollution on the Shortwave Albedo of Clouds, *J. Atmos. Sci.*, 34, 1149–1152, doi:10.1175/1520-0469(1977)034<1149:TIOPOT>2.0.CO;2, 1977.

van der Werf, G. R., Randerson, J. T., Giglio, L., Collatz, G. J., Mu, M., Kasibhatla, P. S., Morton, D. C., DeFries, R. S., Jin, Y., and van Leeuwen, T. T.: Global fire emissions and the contribution of deforestation, savanna, forest, agricultural, and peat fires (1997–2009), *Atmos. Chem. Phys.*, 10, 11707-11735, doi:10.5194/acp-10-11707-2010, 2010.

Wilcox, E. M., Thomas, R. M., Praveen, P. S., Pistone, K., Bender, F. A.-M., and Ramanathan, V.: Black carbon suppresses atmospheric turbulence, Proc. Nat. Acad. Sci., 113, 42, 11794-11799; DOI: 10.1073/pnas.1525746113, 2016.

Wood, R., Leon, D., Lebsock, M., Snider, J., and Clarke, A. D.: Precipitation driving of droplet concentration variability in marine low clouds, J. Geophys. Res., 117, D19210, doi:10.1029/2012JD018305, 2012.

Yamaguchi, T., G. Feingold, J. Kazil,and A. McComiskey, A.: Stratocumulus to cumulus transition in the presence of elevated smoke layers, *Geoph. Res. Lett.*, 42, 10,478–10,485,doi:10.1002/2015GL066544, 2015.

Zhang, J. and Zuidema, P.: ~~Low cloud reduction within~~The diurnal cycle of the smoky marine boundary layer ~~and~~ observed during August in the ~~diurnal cycle~~remote southeast Atlantic, Atmos. Chem. Phys~~. *Discuss.*, https://~~, 19, 14493-14516, doi~~.~~org/10.5194/~~:acp-19-14493-2019~~-448, in review~~, 2019.

Zhou, X. and Ackerman, A. S. and Fridlind, A. M. and Wood, R. and Kollias, P.: Impacts of solar-absorbing aerosol layers on the transition of stratocumulus to trade cumulus clouds, Atmos. Chem. Phys., 17, 20, 12725-12742, doi:10.5194/acp-17-12725-2017, 2017.

Zuidema, P., Sedlacek, A. J. III,Flynn, C., Springston, S.,Delgadillo, R., Zhang, J., et al.: The Ascension Island boundary layer in the remote southeast Atlantic is often smoky. *Geoph. Res. Lett.*, 45, 4456–4465, doi:10.1002/2017GL076926, 2018.

Formatted: Font: Not Italic

Tables

Table 1: Average marine boundary layer (MBL) aerosol concentrations from the UHSAS, CCN activity derived from in-situ CCN measurements (κ_{CCN}) and bulk chemical composition (κ_{AMS}), and characteristic vertical updraft velocity (w^*). Aerosol conditions are classified for each flights as "polluted", "intermediate", or "clean" based on the MBL aerosol concentration.

Flight Number	Date	Pollution Category	Aerosol Number (cm^{-3})	*CFSTGC Operation Mode*	κ_{CCNc}	κ_{AMS}	w^* (ms^{-1})
RF01	12 Aug 17	Polluted	707 ± 104	Both[$]	0.4	-	0.~~45~~44
RF02	13 Aug 17	Polluted	1012 ± 98	Both[$]	0.4	0.4	0.~~39~~40
RF03	15 Aug 17	Intermediate	481 ± 109	SFCA[^]	0.4	0.4	0.~~44~~42
RF08	24 Aug 17	Intermediate	493 ± 40	Both[$]	0.3	0.4	0.~~29~~32
RF09	26 Aug 17	Intermediate	433 ± 34	CF[*]	0.4	0.4	0.~~45~~35
RF10	28 Aug 17	Clean	205 ± 21	CF[*]	0.3	-	0.~~32~~33
RF11	30 Aug 17	Clean	278 ± 24	Both[$]	0.2	0.4	0.~~26~~24
RF12	31 Aug 17	Clean	195 ± 21	CF[*]	0.4	0.4	0.3[#]

[*] CF: Constant Flow operation of the CCN instrument.

[^] SFCA: Scanning Flow CCN Analysis operation of the CCN instrument.

[$] Both operation modes (CF, SFCA) of the CCN instrument were used.

w^*=0.3 ms^{-1} assumed when calculating droplet number. This value was selected based on the pollution category and date, and the average of corresponding w^* determined from RF10, RF11.

Formatted Table

Figures Captions

Figure 1: Map of ORACLES 2017 research flights used in this work, together with aerosol optical thickness (AOT) of the August 2017 plume (Meyer et al., 2015). The inset provides MODIS imagery of savannah fires throughout August 2017. Most flights are in close proximity to the "routine" flight path of due South along 5°E Longitude.

Figure 2: Vertical profiles (altitude in meters) of CCN concentration (cm^{-3}) from 0.1% to 0.4% supersaturation for all flights in this work.

Figure 3: ~~Top panel:~~a) Predicted droplet number (N_d; cm^{-3}) and measured CCN (cm^{-3}) at 0.1% supersaturation as functions of marine boundary layer aerosol concentration (N_a; cm^{-3}) for all flights. ~~Bottom panel:~~b) N_d against N_a in the MBL for all flights, colored by maximum in-cloud supersaturation (S_{max}).

Figure 4: The sensitivity of droplet number to a) aerosol number ($\partial N_d/\partial N_a$), b) characteristic velocity ($\partial N_d/\partial w^*$), and, c) hygroscopicity parameter ($\partial N_d/\partial \kappa$) as functions of N_a (cm^{-3}). The data is clustered using the "polluted", "intermediate", and "clean" groupings of Table 1.

Figure 5: Characteristic velocity, w^*, in the MBL as a function of N_a (cm^{-3}) in the BBOA plume (blue) and in the MBL (red), for each flight.

Formatted: Font color: Auto

Figure 6: N_d^{lim} (cm^{-3}) for each flight as a function of characteristic vertical updraft velocity, w^* (ms^{-1}). Flights are colored by "polluted", "intermediate", and "clean" categories, as defined by MBL concentration. The inset also presents the "asymptotic" activated droplet number (N_d^{lim}; cm^{-3}) for w^* ranging from 0.1 to 0.6 ms^{-1}.

~~**Figure 7:** Spatial context of MBL aerosol for August 2017. Marker size as a function of N_a (cm^{-3}) and color as a function of N_a (cm^{-3}).~~

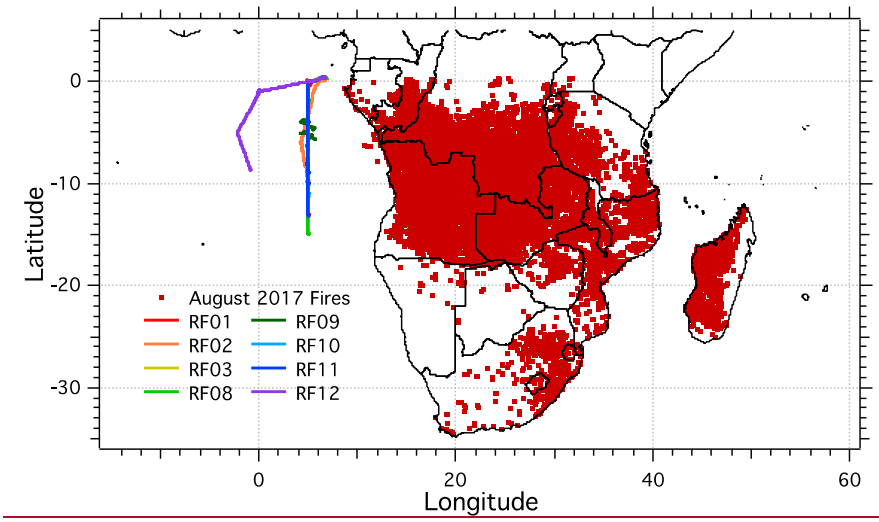

774

775

776

777

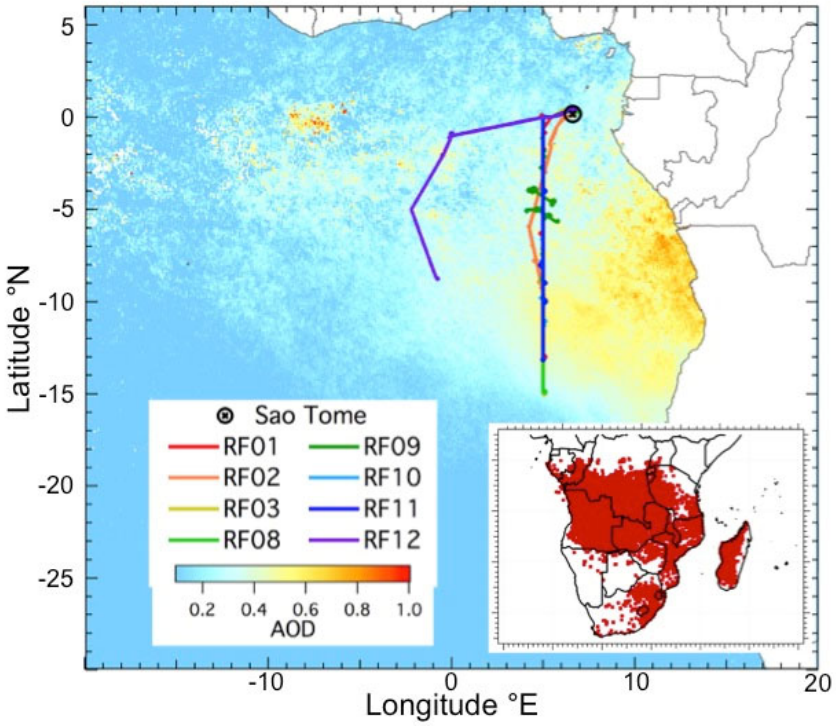
Latitude °N
Longitude °E
5
0
-5
-10
-15
-20
-25
-10
0
10
20
Sao Tome
RF01
RF02
RF03
RF08
RF09
RF10
RF11
RF12
0.2
0.4
0.6
0.8
1.0
AOD

Figure 1

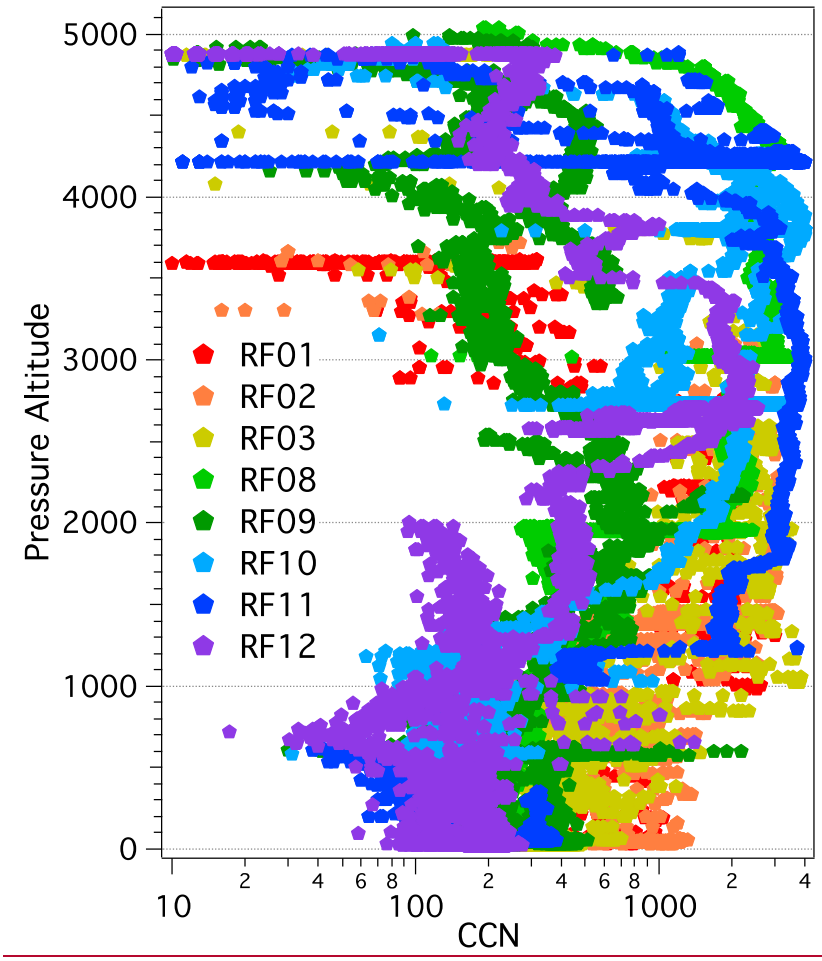
5000
4000
3000
2000
1000
0
Pressure Altitude
RF01
RF02
RF03
RF08
RF09
RF10
RF11
RF12
10
2
4
6
8
100
2
4
6
8
1000
2
4
CCN

782

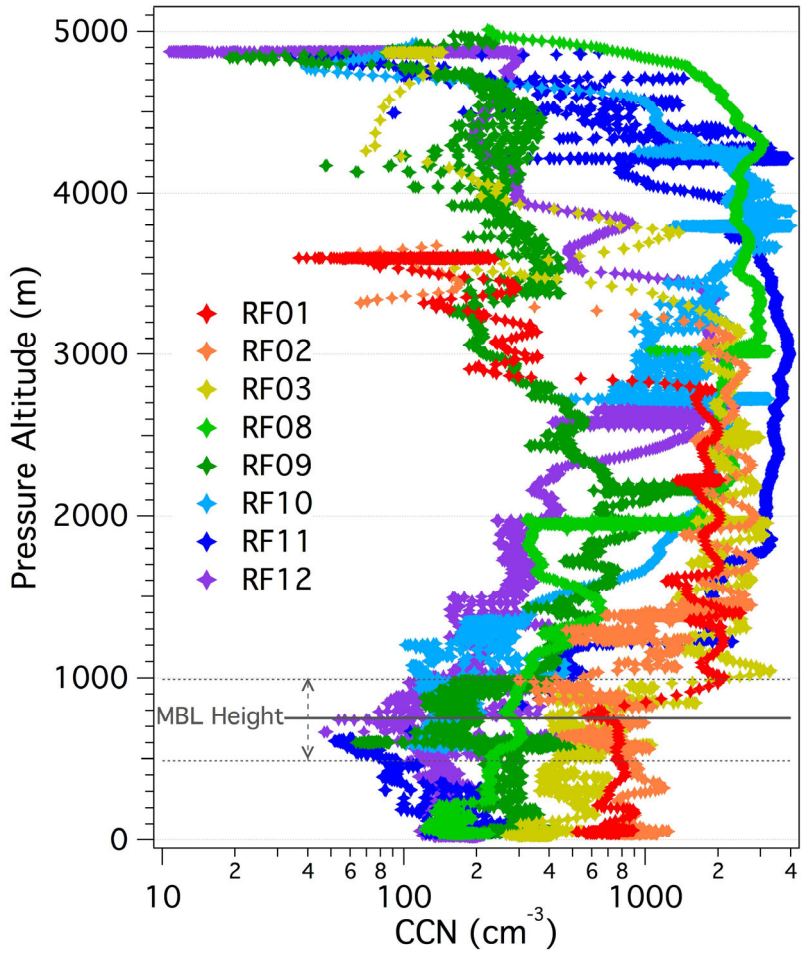
5000
4000
3000
2000
1000
0
Pressure Altitude (m)
RF01
RF02
RF03
RF08
RF09
RF10
RF11
RF12
MBL Height
10
2
4
6
8
100
2
4
6
8
1000
2
4
CCN (cm-3)

Figure 2

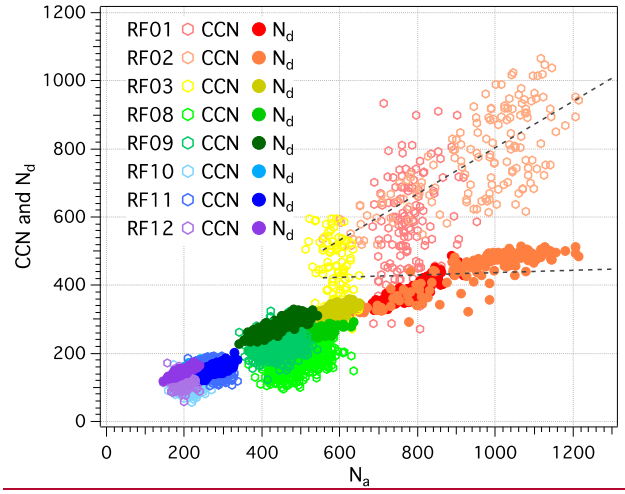
RF01 CCN Nd
RF02 CCN Nd
RF03 CCN Nd
RF08 CCN Nd
RF09 CCN Nd
RF10 CCN Nd
RF11 CCN Nd
RF12 CCN Nd
CCN and Nd
Na
0
200
400
600
800
1000
1200

788

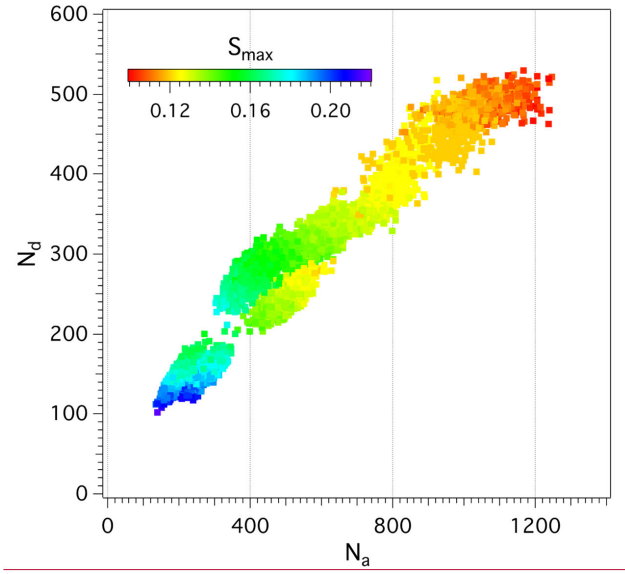
Smax
0.12
0.16
0.20
Nd
Na
0
100
200
300
400
500
600
0
400
800
1200

789
790

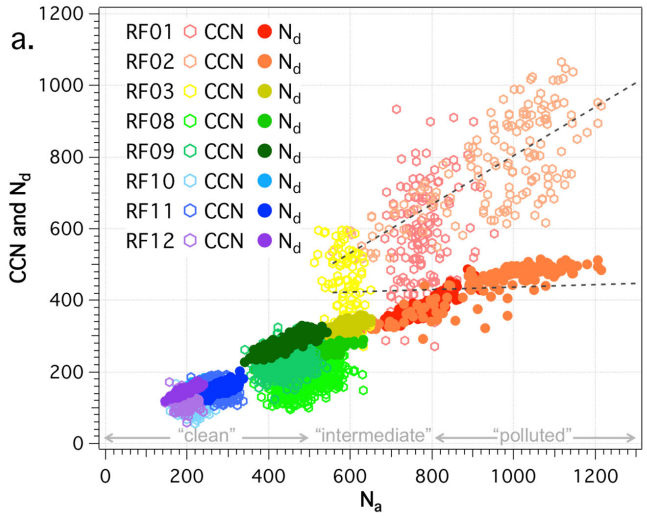
a.
RF01 CCN Nd
RF02 CCN Nd
RF03 CCN Nd
RF08 CCN Nd
RF09 CCN Nd
RF10 CCN Nd
RF11 CCN Nd
RF12 CCN Nd
CCN and Nd
Na
"clean"
"intermediate"
"polluted"
0
200
400
600
800
1000
1200

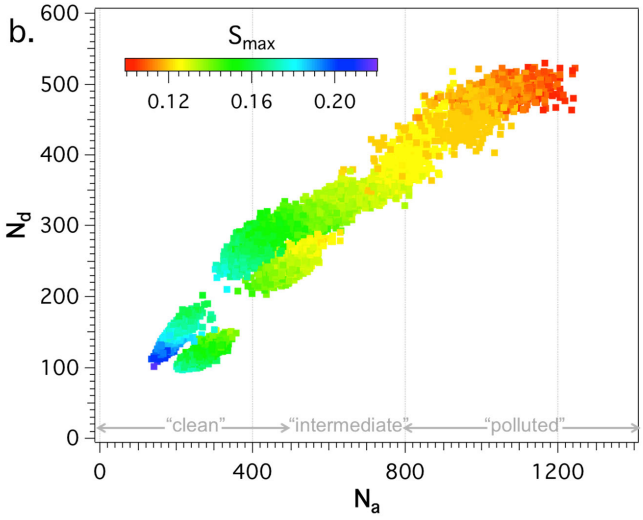
b.
Smax
0.12
0.16
0.20
Nd
Na
"clean"
"intermediate"
"polluted"
0
100
200
300
400
500
600
1200

Figure 3

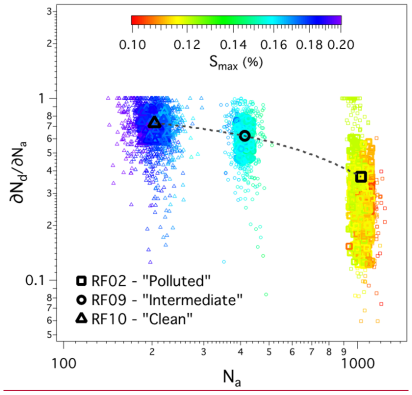
0.10 0.12 0.14 0.16 0.18 0.20
S_{max} (%)
$\partial N_d/\partial N_a$
RF02 - "Polluted"
RF09 - "Intermediate"
RF10 - "Clean"
100
1000
N_a

796

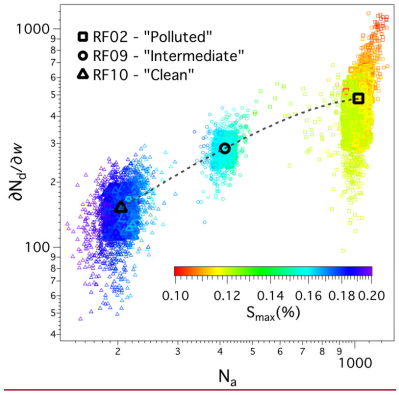
RF02 - "Polluted"
RF09 - "Intermediate"
RF10 - "Clean"
$\partial N_d/\partial w$
0.10 0.12 0.14 0.16 0.18 0.20
S_{max}(%)
1000
N_a

797

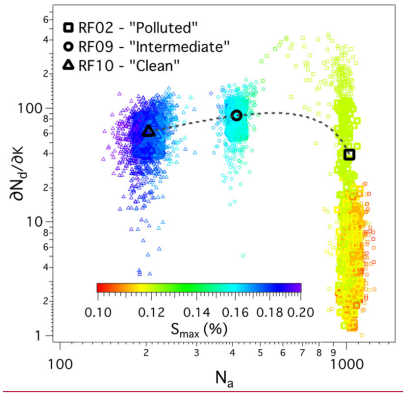
RF02 - "Polluted"
RF09 - "Intermediate"
RF10 - "Clean"
$\partial N_d/\partial K$
0.10 0.12 0.14 0.16 0.18 0.20
S_{max} (%)
100
1000
N_a

798

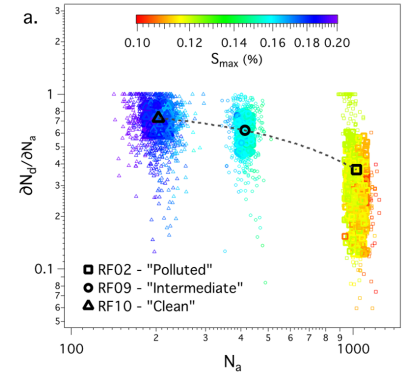
a.
0.10 0.12 0.14 0.16 0.18 0.20
S_{max} (%)
$\partial N_d/\partial N_a$
RF02 - "Polluted"
RF09 - "Intermediate"
RF10 - "Clean"
100
1000
N_a

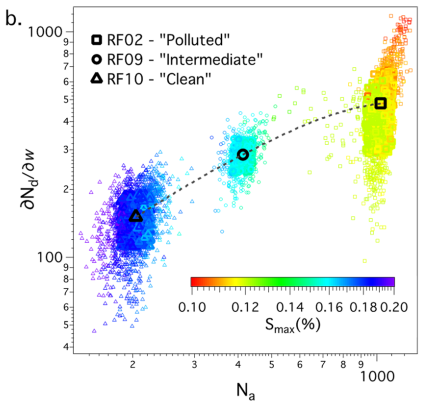
b.
RF02 - "Polluted"
RF09 - "Intermediate"
RF10 - "Clean"
$\partial N_d/\partial w$
0.10 0.12 0.14 0.16 0.18 0.20
S_{max}(%)
1000
N_a

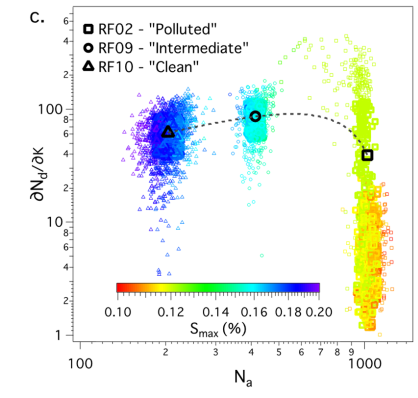
c.
RF02 - "Polluted"
RF09 - "Intermediate"
RF10 - "Clean"
$\partial N_d/\partial K$
0.10 0.12 0.14 0.16 0.18 0.20
S_{max} (%)
100
1000
N_a

Figure 4

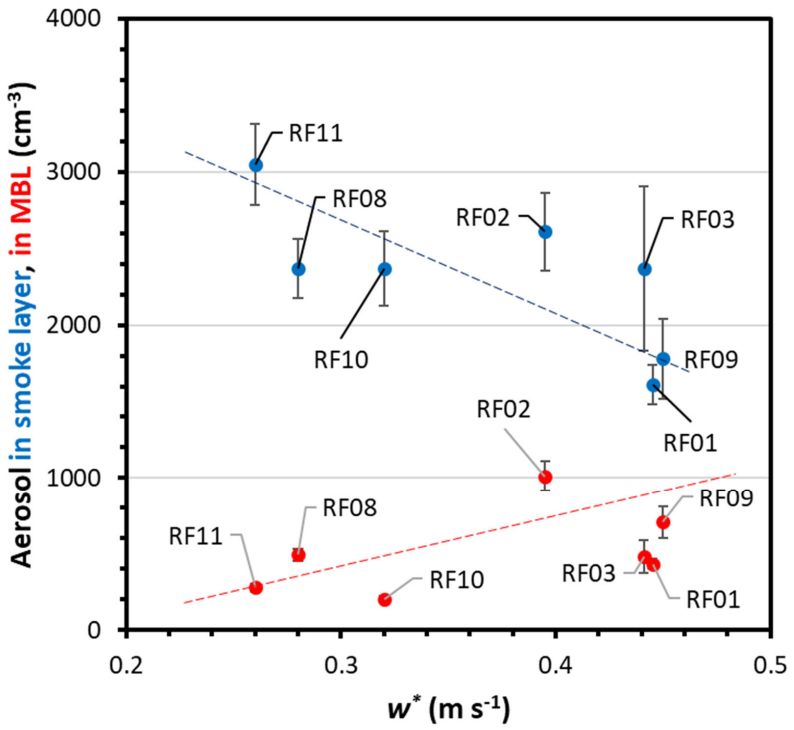
Aerosol in smoke layer, in MBL (cm-3)
4000
3000
2000
1000
0
0.2
0.3
0.4
0.5
w* (m s-1)
RF11
RF08
RF02
RF03
RF10
RF09
RF01
RF02
RF09
RF08
RF11
RF10
RF03
RF01

804

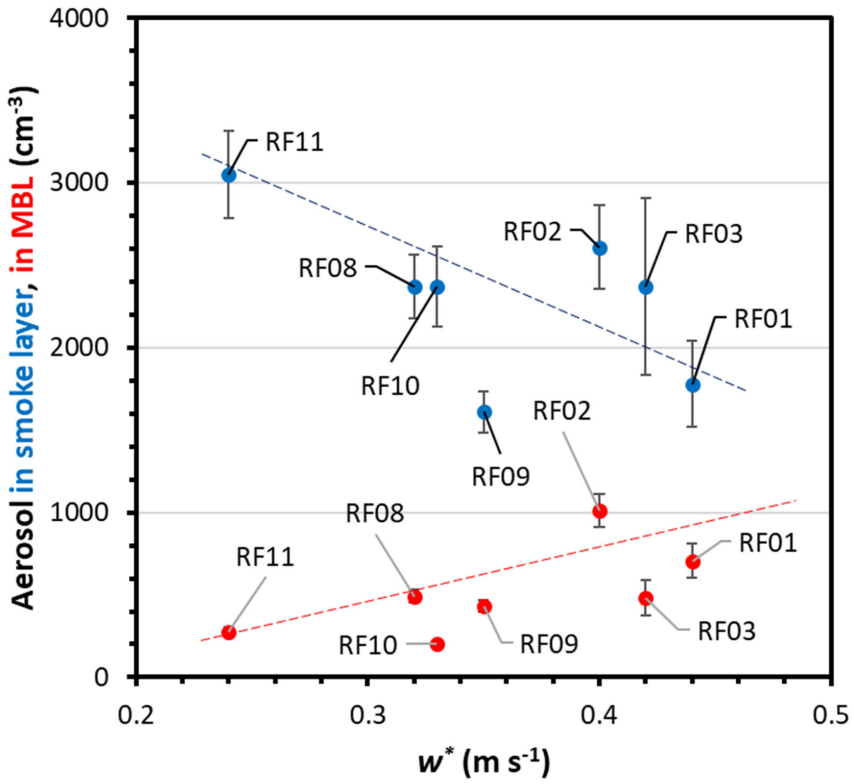

805

806

807 **Figure 5**

808

809

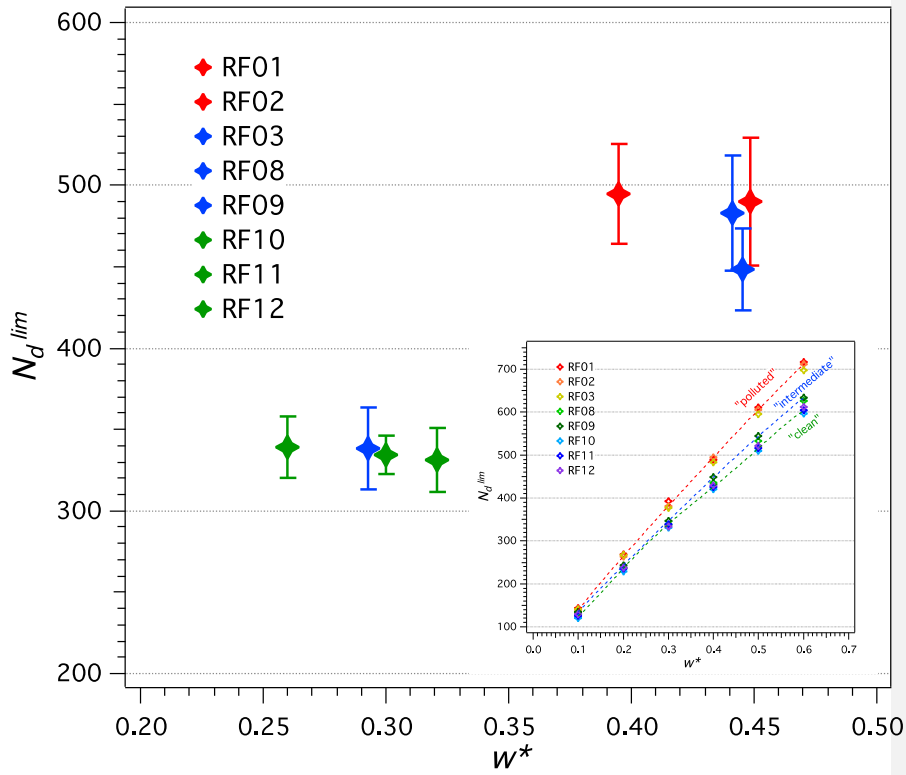
RF01
RF02
RF03
RF08
RF09
RF10
RF11
RF12
N_d^{lim}
w^*
"polluted"
"intermediate"
"clean"

810

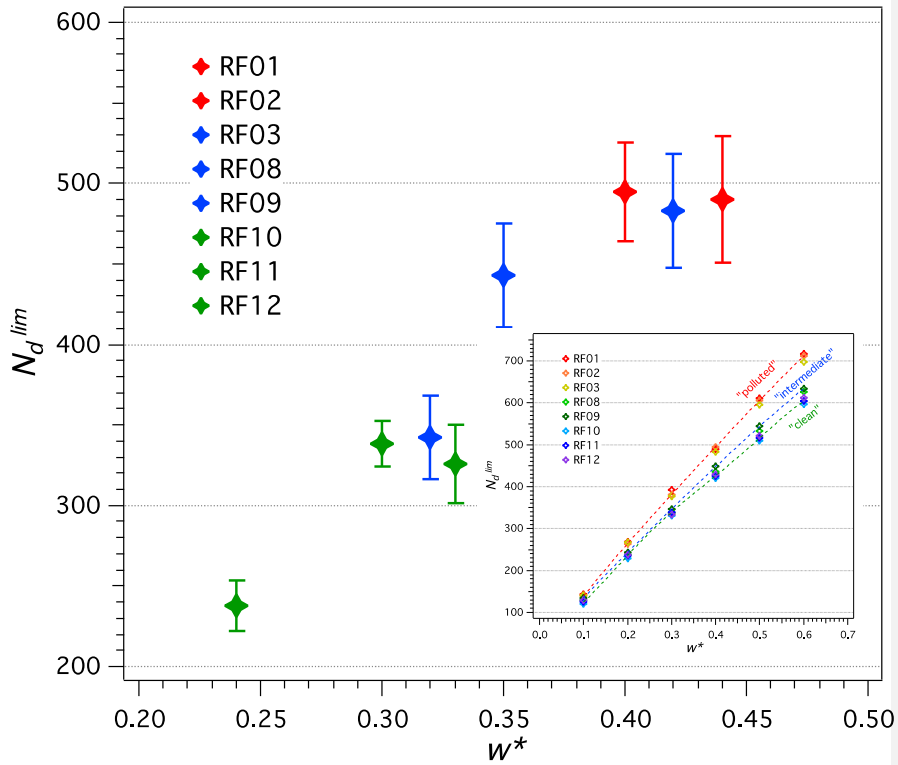
RF01
RF02
RF03
RF08
RF09
RF10
RF11
RF12
N_d^{lim}
w*
"polluted"
"intermediate"
"clean"

Figure 6

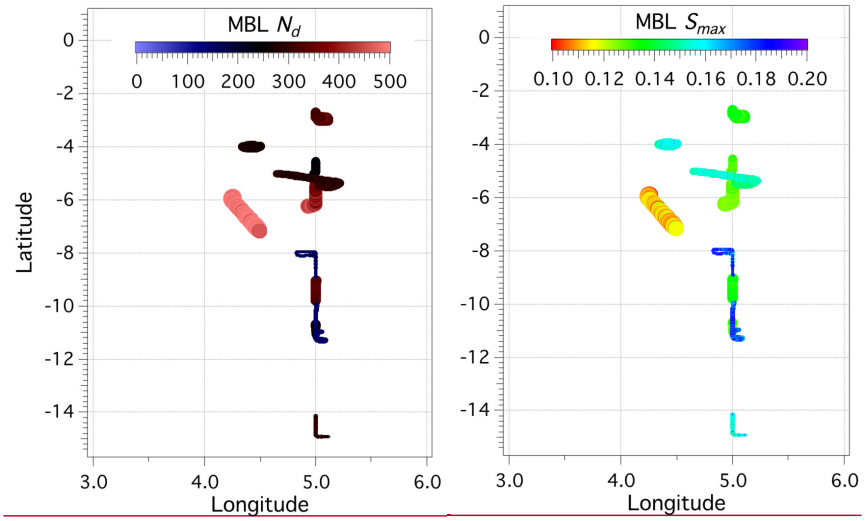

~~Figure 7~~

Formatted: Font: Bold